

Individual-defect electromigration in metal nanobridges

K. S. Ralls, D. C. Ralph, and R. A. Buhrman

School of Applied and Engineering Physics, Cornell University, Ithaca, New York 14853-2501

(Received 20 July 1989)

We have studied electromigration in metal nanobridges sufficiently small that individual-defect motion can be observed in the resistance noise. True electromigration occurs by a very complex process of a "defect glass" evolving in time under an applied bias, rather than by simple diffusion of independent defects. At lower biases, reversible precursors to electromigration provide quantitative information about the electromigration of individual defects. A random energy transfer from the electrons to the defects dominates the expected electromigration-force term, accelerating the electromigration process by heating the defects preferentially above the lattice temperature.

I. INTRODUCTION

The detailed microscopic mechanism of electromigration remains speculative despite considerable theoretical progress in the field, because experiments have measured only average properties in macroscopic samples, such as mean time to failure of a wire or the motion of marker atoms.^{1,2} Here we report results of measurements on metal nanobridges so small that we can actually observe the microscopics of individual electromigration events directly in the resistance fluctuations. In these clean, probably single-crystal samples we find that interactions between defects dominate the defect dynamics. Consequently, electromigration occurs not due to simple diffusion of independent defects, but through a complex relaxation of a strongly interacting "defect glass" under the influence of the applied bias. By examining the reversible fluctuation precursors to electromigration we are able to make quantitative measurements of electromigration parameters on *individual* defects. In these high-field, very-high-current-density devices we find that inelastic electron-defect collisions play a major role in the electromigration behavior through the excitation of the defects to effective temperatures above that of the lattice. This inelastic defect scattering enhances the random fluctuation rates of the local defect glass and thereby accelerates the electromigration process.

Electromigration refers to the net motion of atomic defects within a material that results when a current is passed through the sample. The driving force for electromigration is typically divided into two components: the direct force due to the bulk electric field acting on the defect and the so-called "electron-wind force" due to momentum transfer from the electrons to the defect.³ Assuming that this wind force is proportional to the electron current, one can write the total force on the defect as $\mathbf{F} = Z_{\text{bare}} e \mathbf{E} = \mathbf{F}_{\text{wind}} = Z^* e \mathbf{E}$, where the effective valence Z^* is composed of the sum of the nominal valence of the defect and an apparent valence due to the electron wind force. Z^* can vary dramatically from the nominal valence, even carrying the opposite sign for free-electron metals,³ indicating that the dynamic

electron-defect interactions are often dominant. Determination of the nominal and effective valences is the focus of much theoretical and experimental research. A fair amount of controversy also exists as to the appropriate value for the bulk electric field,⁴⁻⁶ for, as Landauer pointed out,⁷ the actual electric field in a conductor is zero, except near the defects that produce the finite sample resistance.

The Fiks-Huntington ballistic model of electromigration presents the simplest picture of electromigration,^{1,8} in which one assumes both a free-electron-gas model and that all of the momentum lost by scattered electrons is transferred to the defect. The ballistic model is appealing because of its simplicity, but, as Bosvieux and Friedel pointed out,⁴ a different approach is required to go beyond the free-electron model. In particular, because a defect scatters the conduction electrons, an applied current induces a charge polarization about the defect. This dynamical screening is the source of the electron-wind force. Many researchers have performed quite sophisticated dynamical screening calculations of the electron-wind force^{4,9-13} given by

$$\mathbf{F} = - \int \delta n(\mathbf{r}) \frac{dU}{d\mathbf{R}} d^3r, \quad (1)$$

where δn is the change in electron density under an applied current, U is the electron-defect interaction potential, and \mathbf{R} is the position of the defect. These calculations reveal that the simple ballistic model can be in error by as much as an order of magnitude in comparison to more accurate calculations. However, because the precise nature of the defects in our samples is unknown, the ballistic model is sufficient for obtaining estimates of expected electromigration parameters to compare with our experimental results.

II. EXPERIMENTAL TECHNIQUE

Nanobridges are fabricated by using electron-beam lithography to pattern a 40–100-nm hole in poly(methyl methacrylate) (PMMA) on a 50-nm suspended Si_3N_4 membrane, and then using a reactive ion etch to transfer

the pattern to the Si_3N_4 . Next, the sample is rotated to expose both sides while metal is evaporated, forming the bridge region in a single processing step. Scanning-electron-microscope studies of arrays of such holes show that while the openings on the patterned side are about 40 nm, the openings on the far side are much smaller. Indeed, our samples are so resistive, $5 < R < 200 \Omega$, that the far-side opening must be small enough to dominate the sample resistance. Figure 1(a) shows a schematic of a 25- Ω nanobridge to scale. Measurements to date have been performed on copper, aluminum, and palladium nanobridges.

Copper and aluminum devices are characterized using point-contact spectroscopy, in which the second derivative of the low-temperature I - V characteristic for a constriction that is small compared to the electron mean free path yields the phonon density of states times the electron-phonon coupling strength.¹⁴ Figure 1(b) shows the phonon spectrum for a 15- Ω copper device taken at 4.2 K. High-quality phonon spectra such as this confirm that ballistic transport dominates in these nanobridges, and suggest that the nanobridge is spanned by a single crystallite, as is also indicated by transmission-electron-microscope examination of test specimens formed in an identical manner. Because these samples are in the ballistic-transport regime at low temperature, we can estimate their size based on the resistance for a ballistic constriction,

$$R \sim 4\rho\lambda/3\pi a^2, \quad (2)$$

where ρ is the resistivity, λ the electron mean free path, and a the constriction radius. Note that this resistance is independent of the electron mean free path, as $\rho \propto 1/\lambda$. Our palladium samples have an elastic mean-free-path

length of about 20 nm, 10 times smaller than for our copper or aluminum samples, and they are therefore not fully ballistic at low temperatures. However, they are fabricated the same way as nanobridges of other materials, so we can use the bulk resistivity and a combination of the ballistic resistance and the ordinary spreading resistance for a constriction, $\rho/2a$, to estimate their sample size. These samples are truly microscopic; a 100- Ω copper nanobridge is 10–20 atoms wide.

Changes in the arrangement of atoms in the constriction are monitored by real-time noise measurements, performed with the sample as one arm of a dc bridge. A battery is used to current-bias the sample, and then the voltage across the arms of the bridge is amplified by a LT1028 differential amplifier, and then by a PAR 113 amplifier. The amplified signal is then sent to a tape recorder, digitizer, or computer for storage and analysis. Measured resistance changes range from 0.02 to 0.5 % of the sample resistance, measured time scales from 10^{-4} to 10^1 sec.

Sample biases used in this study range from 1 to 500 mV, with true electromigration, in which the sample resistance changes slowly but permanently, occurring at the higher biases. The voltage at which electromigration begins in a given nanobridge correlates with the temperature, sample resistance, and nanobridge material, ranging from ~ 30 mV for a 5- Ω aluminum sample at room temperature to ~ 500 mV for a 100- Ω copper sample at 4.2 K. These nanobridges are quite stable at a 10-mV bias at 300 K; this is quite remarkable because the current density at the center of a nanobridge under these conditions is $J \sim 10^8$ A/cm² and the electric field strength is $E \sim 10^4$ V/cm. These are both more than an order of magnitude higher than sustainable in polycrystalline thin-film resistors of copper or aluminum, where diffusion along grain boundaries is believed to dominate mass transport. Electromigration in our smallest nanobridges does not occur until the current density is nearly 10^{10} A/cm².

III. INDIVIDUAL DEFECT NOISE

The 50–200- Ω nanobridges are so small that we can observe the resistive effect of individual defects fluctuating between metastable configurations, as has been described for copper nanobridges in more detail elsewhere.¹⁵ First, we discuss the behavior of the noise at low sample biases, where the behavior of the noise does not have any bias dependence. The bias dependence of the noise is discussed in Sec. IV. For temperatures $20 < T < 150$ K the individual-defect noise is stable in time and, most typically, the resistance switches randomly back and forth between two values as shown in Fig. 2. The average time spent in the high- or low-resistance state is well described by thermally activated behavior,

$$\tau \sim \tau_0 e^{\epsilon/kT}, \quad (3)$$

where τ_0^{-1} is the attempt rate and ϵ is the activation energy. In general, τ_0 and ϵ differ for the two states, although they must be similar in size in order for the fluctuation to be observable. Measured values of $\tau_0 \sim 10^{-11}$ – 10^{-15} sec

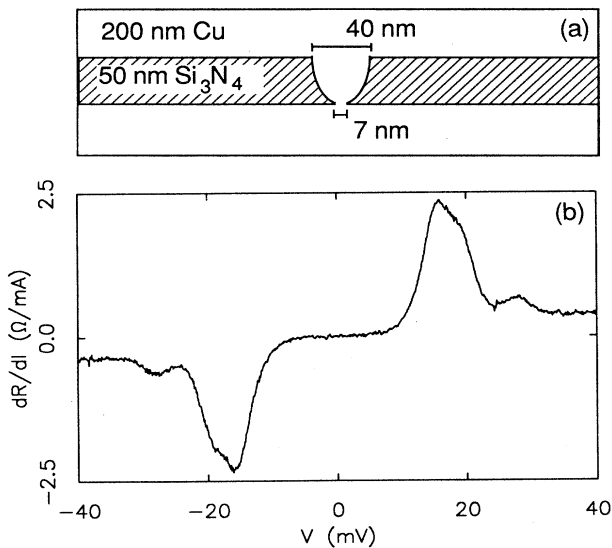


FIG. 1. (a) Cross-sectional schematic of a 25- Ω nanobridge, to scale. (b) Typical phonon spectrum for a 15- Ω copper nanobridge. Such a high-quality phonon spectrum confirms that transport is ballistic in this device.

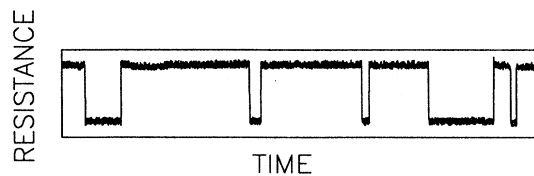


FIG. 2. Simplest sort of low-frequency noise seen at low temperatures ($T < 150$ K) consisting of discrete resistance fluctuations with time, due to the reconfiguration of an individual defect. The time scale can be anywhere in the experimental bandwidth, 10^{-4} – 10^1 sec; typical fluctuation magnitudes are $\sim 0.1\%$ of the total resistance.

and scattering-cross-section changes $\Delta\sigma \sim 0.1 \text{ nm}^2$, inferred from the measured resistance changes, support individual atomic-sized defect motion as the origin of this noise. The activation energies for the low-temperature fluctuations, $\epsilon \sim 30$ – 300 meV, indicate that these metastable defects are comparatively weakly bound. It should be noted that these activation energies reflect the measurement temperatures, with the smallest energies corresponding to fluctuations observed at the lowest temperatures.

At higher temperatures, but still at low sample bias, more defect fluctuations become active, and interactions between defects, in which the reconfiguration of one defect affects the fluctuation rate of another, become more and more common. (In some rare instances, the reconfiguration of one defect affects the amplitude of another defect fluctuation. Such an interaction can occur if the defects are within an electron screening length of each other; the rarity of this type of interaction indicates that, in general, the defects are interacting over a distance that is much greater than an electron screening length.) Above $T \sim 150$ K interactions between defects dominate, leading to a complex noise signal still composed of discrete resistance fluctuations, but with the characteristic times, amplitudes and number of active fluctuators constantly changing in time. Noise snapshots illustrating such behavior for a $90\text{-}\Omega$ copper nanobridge at 300 K are shown in Fig. 3.

Even though the copper is quite crystalline, we find that it is more appropriate to consider the fluctuations as arising from a “defect glass” system which, above ~ 150 K (for copper), has melted, and is wandering in a very complicated potential in an attempt to anneal to equilibrium. This view is further supported by the fact that, in general, the two-level fluctuators (TLF’s) observed at low temperatures change with each temperature cycling of the sample, even though there is no overall annealing of the noise nor measurable change in the device conductance. Thus, below ~ 150 K the system is frozen into a particular configuration of accessible double-well potentials that determine the possible low-temperature dynamics of defect fluctuations. This configuration is determined by what part of the complex potential the system freezes into upon cooling past the effective defect glass melting point.

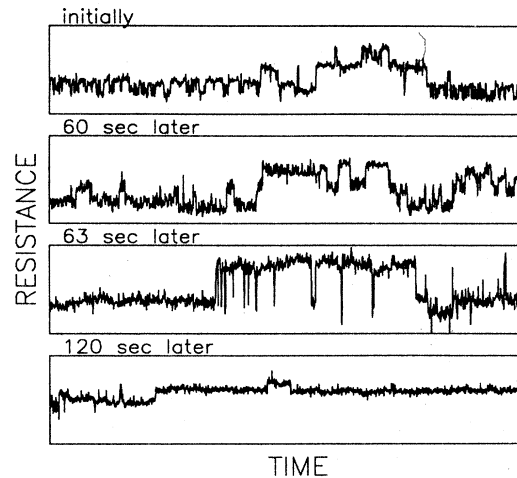


FIG. 3. Resistance vs time for a $90\text{-}\Omega$ nanobridge (≥ 3.5 nm across) at 300 K showing that although discrete resistance fluctuations still occur at high temperatures, interactions between defect fluctuations cause the noise signal to evolve in time. Each noise snapshot is about 0.2 sec long.

We stress that even though our samples are high-quality crystalline thin-film materials with relatively long defect scattering lengths ($\lambda \sim 200$ nm for the copper films), there is apparently no such thing as an independent fluctuating defect. Interactions between defects are sufficiently strong that the defect system must be considered as a whole. We might expect this noise to be due to the reversible motion of a simple, relatively independent, defect that is interacting weakly with local disorder, such as a vacancy. We find, however, that the individual defect noise we observe is best ascribed to a local fluctuation over a barrier between double wells of the entire defect potential.

Apparently, most of the scatterers within the nanobridge are capable of fluctuating. Resistance measurements of a “bulk” portion of the copper film yield an impurity mean free path of ~ 200 nm, which gives an average defect spacing of ~ 3 nm, assuming atomic dimensions for the defect cross section. The defect density within the nanobridge may be somewhat higher than in the bulk of the film due to surface and thermal strains, but the low-temperature point-contact spectrum establishes that the defect density there is still of a similar order of magnitude as in the bulk film. We find that on average there is about one defect fluctuation occurring at any given time within the experimental bandwidth for the noise signal of Fig. 3, indicating that a significant fraction of all of the defects within the nanobridge region are fluctuating at room temperature.

These defects are exerting significant interactions between each other, over distances of order the average defect spacing of 3 nm or greater. The long-range nature of this interaction suggests that it occurs through the defect strain field, which in the long-wavelength limit varies as $1/r^3$. The mean activation energy of the defect fluctuations at 300 K is estimated as $\epsilon \sim 0.5$ – 0.75 eV. Assum-

ing a fluctuation attempt rate equal to the mean of the measured values, $\tau_0^{-1} \sim 10^{13} \text{ sec}^{-1}$, significant modulation of the mean frequency of a defect fluctuation at 300 K requires a change in activation energy of $\delta\epsilon \geq 50 \text{ meV}$, while moving the fluctuation completely out of the experimental bandwidth, as is often seen, can require $\delta\epsilon \geq 200 \text{ meV}$. Thus, whatever the interaction mechanism, it is sufficiently strong to completely dominate the defect dynamics whenever a small number of such defects are active in a volume of the order of $(3 \text{ nm})^3$.

IV. ELECTROMIGRATION

A. Irreversible electromigration

As a function of increasing bias voltage, the discrete resistance noise observed for $T < 150 \text{ K}$ is strikingly similar to that observed with increasing temperature: when the sample bias is raised, the two mean rates of the stable TLF's are both seen to increase, and eventually the fluctuations leave the experimental bandwidth. New TLF's pass through the experimental bandwidth (0.1 Hz–10 kHz) until at a high enough sample bias interactions between defects dominate, and the noise signal wanders in time in a manner similar to that seen at high T . However, the spacing and order in which the two-level fluctuations are observed is not identical for increasing T and V and, as will be shown later, the voltage dependence of the defect fluctuation rates is not due to straightforward sample heating.

As the sample bias is raised further, well past the point where the noise signal begins to vary in time, the sample resistance begins to change irreversibly as shown in Fig. 4 for a 120- Ω copper sample at 77 K and 250 mV. The plot in Fig. 4(a) shows the net resistance change of 3% over a fairly long time, 30 sec. More interesting are the time expansions of this signal shown in Fig. 4(b), which show that the resistance dynamics are still dominated by

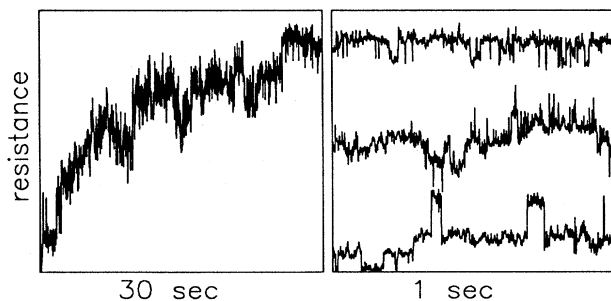


FIG. 4. (a) Resistance of a 120- Ω nanobridge ($\geq 3.0 \text{ nm}$ across) changing by $\sim 3\%$ under an applied bias of 250 mV. (b) Time expansions of (a) showing that electromigration is dominated by discrete resistance fluctuations of the wandering nature characteristic of high temperatures. The applied voltage biases the “defect glass,” encouraging net atomic motion, and accelerates the electromigration process by preferentially heating the defects above the lattice temperature.

discrete resistance fluctuations, but that instead of wandering about a mean resistance, the probability of specific fluctuations occurring is biased, so that the resistance changes permanently. With care, electromigration can increase the resistance of a nanobridge by a factor of 20, although the sample resistance is as likely to decrease as it is to increase under the applied bias.

Data such as those seen in Fig. 4 present a very different qualitative picture of electromigration than that of simple diffusion of defects. We find instead a situation in which the “defect glass” described above responds to the applied bias in a most complex manner. Many fluctuation modes of this defect glass in its complex and constantly evolving potential must be excited before the system has access to net atomic motion, as indicated by the fact that net electromigration does not occur until the sample is well into the regime where the noise signal varies in time. Net atomic motion is occurring by a very tortuous process where, for example, a given defect reconfigures reversibly for a while, and then a different path for motion is opened up due to the reconfiguration of another defect. If this second fluctuation has its available configurations changed by the motion of a third defect, and so on, the system may never return to a state where the initial fluctuation can recur, and an irreversible change is accomplished.

We see that the applied voltage and current have two major effects on this process of defect random walk in a complex fluctuating and evolving potential. First, the applied field and the electron-wind force bias the fluctuation process so that certain defect configurations are more probable than they are at zero applied voltage, thus promoting net atomic motion. (A similar biasing effect can result from thermal stress-induced strain in the metal.¹⁶) Second, the applied voltage strongly enhances the individual defect fluctuation rates, greatly increasing the occurrence of those local defect configurations that can facilitate net atomic motion and thereby accelerate electromigration.

B. Reversible electromigration

The details of these two effects can be established by examining the response of individual defect fluctuations to the applied bias, since even at voltages below those at which appreciable net electromigration occurs one would expect the defects to be influenced by the electric field and electron-wind force, just not strongly enough to produce long-range atomic motion. The presence of stable TLF's indicates that there are only a few low-energy barriers to atomic motion accessible for any given temperature and voltage. Consequently, the system can only “electromigrate” back and forth between a few metastable defect configurations, and the influence of electromigration forces on the defect dynamics is merely a precursor to true electromigration. However, because this process is reversible and stable over laboratory time scales, we can obtain quantitative data for the voltage and temperature dependence of the average time spent by a single defect in each of its two configurations. Thus we can actually measure the electromigration behavior of *individu-*

al defects by studying the voltage and temperature dynamics of stable TLF's. Figure 5 shows such data of the log of the average time τ spent in one defect configuration as a function of voltage at several temperatures for a single defect reconfiguring in (a) an aluminum and (b) a copper nanobridge. As can be seen, $\log_{10}(\tau)$ versus V does have an antisymmetric component that results in an offset of the data about zero voltage. In terms of Eq. (3), this behavior suggests that the defect fluctuation activation energy ε is modified by the bias as

$$\varepsilon = \varepsilon_0 - \zeta V. \quad (4)$$

This is the expected combined results of the two electromigration force terms on the defect.

However, the most striking and dominant feature of the data is the large, symmetric variation of $\log_{10}(\tau)$ versus V . This reflects the increase in the TLF fluctuation rates, regardless of defect configuration or the direc-

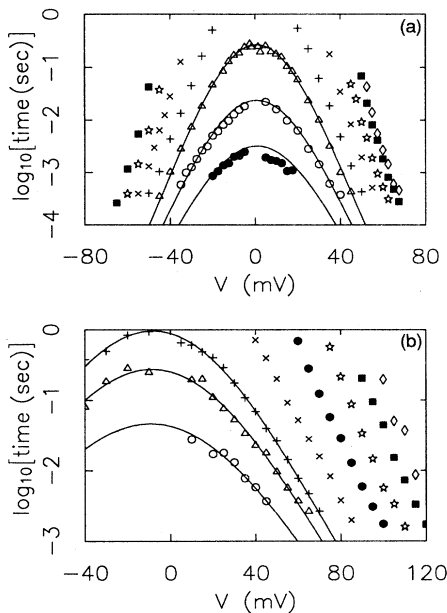


FIG. 5. (a) Voltage dependence of the time spent in one defect configuration for several temperatures for a defect in an aluminum nanobridge: \bullet , $T=118$ K; \circ , $T=108$ K; \triangle , $T=98$ K; $+$, $T=89$ K; \times , $T=77$ K; \star , $T=60$ K; \blacksquare , $T=39$ K; \diamond , $T=19$ K. The large symmetric dependence is roughly quadratic at low biases, as shown by the fit. This behavior is due to random energy transfer from the electrons to the defect, and dominates the expected electromigration force term. (b) Voltage dependence of the time spent in one defect configuration for several temperatures for a defect in a copper nanobridge: \circ , $T=115$ K; \triangle , $T=106$ K; $+$, $T=101$ K; \times , $T=90$ K; \bullet , $T=77$ K; \star , $T=61$ K; \blacksquare , $T=44$ K; \diamond , $T=4$ K. Note again the large symmetric term that is quadratic in voltage at low biases. The offset of the data about zero voltage is due to the electromigration force term.

tion of the samples bias, as described above. At low voltages this symmetric component is roughly quadratic in voltage, but at higher voltages, and, consequently, at lower temperature due to the limited experimental bandwidth, the data show a slight curve in the opposite direction. For the low-temperature, high-voltage data the fluctuation rate becomes rapidly temperature independent, as shown in Fig. 6. This increase in the defect fluctuation rate for both directions of sample bias suggests that the defect temperature is increasing with increasing voltage, so that Eq. (3) should be modified by replacing the temperature T with some effective defect temperature T_d .

While this voltage effect has the character of heating the defect, we emphasize that the bias contribution to the effective temperature T_d is *not* due simply to overall sample heating. This is demonstrated clearly in Fig. 7, which shows the duty cycle $\tau_1/(\tau_1+\tau_2)$ of a TLF as a function of the average time spent in the high-resistance state τ_1 for various temperatures at low voltage, and for various positive and negative high voltages at fixed temperature. As long as the linear electromigration term is small, τ_1 serves essentially as an indication of the effective temperature of the defect in the high-resistance state. Because the duty cycle at low voltages is fairly temperature independent, overall sample heating due to increasing sample bias should produce a constant duty cycle equal to that found at low voltages. We find that the duty cycle as a function of τ_1 is significantly different at high voltage than it is at low voltage. The linear electromigration term would increase the duty cycle for one bias direction and decrease it for the other direction. But we see instead that at low voltages the duty cycle is roughly 50% ($\tau_1 \sim \tau_2$), and the defect spends about the same amount of time in the high- and low-resistance states for all temperatures, while at both positive and negative high voltages the duty cycle is about 70% ($\tau_1 > \tau_2$). Thus, at high sample bias the defect is at a higher effective temperature in its low-resistance state than it is in its high-resistance state. Although the defect is "heated" in both

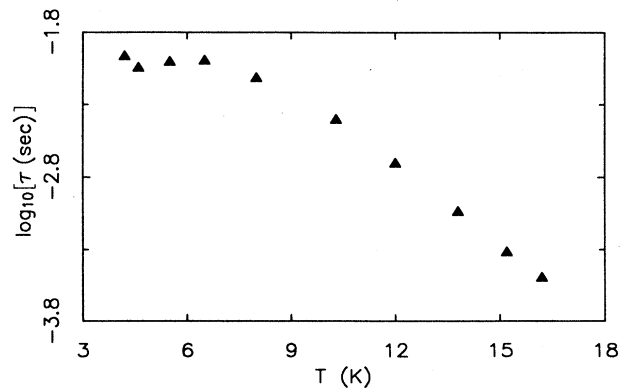


FIG. 6. Fluctuation rate of a defect at low temperatures observed at 19 mV in a copper nanobridge. Notice that the fluctuation time becomes independent of T at low temperatures.

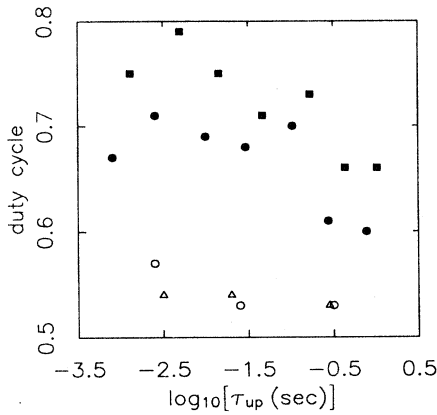


FIG. 7. Duty cycle of a two-level fluctuation as a function of the average time spent in one defect configuration. Note that the duty cycle for both positive (■) and negative (●) high voltage, 20–50 mV, at fixed temperature, 89 K (solid symbols), is different from that observed for all temperatures, 100–120 K, at low voltages, ± 5 mV (open symbols). This means that the increase in the defect's effective temperature with increasing sample bias cannot be due to overall sample heating, as high voltage "heats" the defect to a different effective temperature depending on which configuration it is in.

configurations by the bias, this "heating" results in a different effective temperature depending on which configuration the defect is in. Thus, this effect cannot be due simply to overall sample heating, proving that the defect is being excited preferentially above the lattice temperature.

V. RESULTS AND DISCUSSION

A. Linear force term

With the modifications indicated above, the mean lifetimes of the TLF's are now given by

$$\tau = \tau_0 e^{(\epsilon - \zeta V)/kT_d} \quad (5)$$

As illustrated in Fig. 6, we find that at higher temperatures Eq. (5) fits the data quite successfully if we choose $T_d = T + \theta V^2$. This allows us to obtain values for τ_0 , ϵ , and ζ from the low-voltage data, which can then be used to calculate T_d . Table I lists measured values of the parameters τ_0 , ϵ , and ζ for four defects studied in copper, aluminum, and palladium nanobridges, with data for the same defect in each of its two configurations for three of these defects. We find that defects in all three materials have comparable electromigration parameters, with $\zeta \sim 0.1$ meV/mV. It is quite interesting that we cannot distinguish a defect in copper from one in aluminum or palladium based on its voltage- and temperature-dependent behavior. This means that individual defects of a given activation energy electromigrate similarly in the three materials, and yet we find that it is substantially easier to change the resistance of aluminum nanobridges by electromigration than for copper nanobridges. For example a 5- Ω aluminum nanobridge at 300 K will change resistance under a bias as low as 30 mV, while a 5- Ω copper nanobridge at 300 K is typically stable until a bias of about 90 mV. We conclude that the aluminum nanobridges change resistance more easily than comparable copper nanobridges because of a difference in the distribution of defect activation energies for the two materials, rather than due to an intrinsically different electromigration process.

We will now discuss these results in the context of the ballistic model of electromigration outlined above. We first note that the electromigration forces in a point contact have been discussed previously by Sorbello,¹⁷ but his result for the wind-force term is not derived in terms of individual defect parameters, and thus differs in detail from that discussed here. We begin with the effect of both the electric field and the electron-wind force on the fluctuating defects which, because these metal nanobridges are essentially linear devices, combine to modify the activation energy ϵ of the defect fluctuations as given by Eq. (4). In a ballistic point contact the bulk electric

TABLE I. Measured electromigration parameters for four defects, characterized by an attempt time τ_0 and an activation energy ϵ , in copper, aluminum, and palladium nanobridges. For three of the defects the electromigration parameters are given for the defect in each of its two configurations. ζ is the linear electromigration force term, α reflects the relative coupling of the defect to the electrons and the lattice, and z/a is the distance of the defect from the center of the device divided by the radius of the device.

Material	R (Ω)	τ_0 (sec)	ϵ (meV)	ζ (meV/mV)	Z^*	α	ω_d	z/a
copper	90	$10^{-11.1}$	73	0.06	0.7	1.8	3×10^{13}	1.3
		$10^{-11.4}$	75	0.05	-0.6	2.0	3×10^{13}	1.3
copper	70	$10^{-10.5}$	210	0.173	2.4	2.0	10^{13}	1.3
aluminum	115	$10^{-11.8}$	220	-0.029	-0.3	1.8	10^{13}	0
		$10^{-11.8}$	220	-0.053	0.6	1.6	10^{13}	0
palladium	250	10^{-12}	175	0.040	0.3	1.8 ^a	10^{13}	0 ^a
		10^{-15}	220	-0.030	0.2	1.8 ^a	10^{13}	0 ^a

^aSee remarks in text concerning these values.

field is also the local electric field seen by the defect since the effect of the geometry dominates that of the impurity scattering. The field is roughly $|\mathbf{E}| \approx V/2a$ at the center of the contact, so that the size of the direct force is

$$|\mathbf{F}_d| \approx eZ(V/2a). \quad (6)$$

This allows an estimate of the electric-field-induced change in the effective activation energy,

$$\delta\varepsilon_d \approx \mathbf{d} \cdot \mathbf{F}_d, \quad (7)$$

where \mathbf{d} is the configuration jump displacement vector for the defect. We can estimate an upper bound for the electron-wind contribution to the linear term by the product of the maximum possible momentum transfer from a single electron, the rate of electron-defect collisions, and the jump distance d . This yields

$$\delta\varepsilon_w = 2mv_F \mathbf{d} \cdot (\mathbf{J}\sigma/e), \quad (8)$$

where \mathbf{J} is electron current density, m the effective electron mass, v_F the Fermi velocity, and σ the scattering cross section for this process. Thus we have that an upper bound on each contribution to the defect activation energy, assuming a jump along the direction of the field, is

$$\begin{aligned} \delta\varepsilon &\equiv (\zeta V)_{\text{wind}} \leq (2mv_F)(J\sigma/e)d, \\ (\zeta V)_{\text{field}} &\leq eZ(V/2a)d. \end{aligned} \quad (9)$$

Notice that the size of the wind force relative to the direct force depends on the bare valence of the defect Z , the nanobridge radius a , and the defect scattering cross section σ such that

$$F_w/F_d \propto a\sigma/Z. \quad (10)$$

Thus, the smaller the nanobridge, the larger the relative size of the direct force.

Comparison of Eq. (9) to the measured values of ζ can be made by estimating the size of the nanobridge based on the ballistic resistance; a 100- Ω copper device is about 3.4 nm across. A configurational jump distance of more than a lattice spacing seems unlikely, so if the largest ζ values observed, $\zeta \sim 0.35$ meV/mV, were strictly due to the electric field, this would imply that the nominal valence $Z = 2a\zeta/d \sim 4$. In estimating the size of the wind force we choose a jump distance of a lattice spacing, $d \sim 3 \times 10^{-10}$ m, and a scattering cross section equal to the typical observed scattering-cross-section change, $\sigma \sim 10^{-19}$ m², resulting in a contribution to the linear parameter of $\zeta \sim 3$ meV/mV. These calculations show that the wind-force term could easily dominate that due to the bulk electric field, but given the unknown nature of the defects being studied, we cannot determine whether or not this is true.

Table I also lists the values of ζ converted into effective valences, assuming that the defect jumps in a straight line along the direction of the field, $eZ^* = \Delta\varepsilon/\mathbf{d} \cdot \mathbf{E} = 2a\zeta/d$, where d can be positive or negative. For a straight-line hop the jump displacement vector \mathbf{d} changes sign when the defect changes configuration, so once we assume the sign of the effective valence for one configuration, the

sign is fixed by the measurement for the other configuration. For $d \sim 3 \times 10^{-10}$ m we find effective valences that are plausible for atomic-size defects, $Z^* \sim 1$. Note that when ζ is recast as an effective valence, we find the somewhat curious result that the effective valence of the defect can change sign when the defect changes its configuration. That is, the activation energy to motion is lowered by the same sign bias for a defect in each of its configurations. This behavior is quite reasonable when considered within the framework of a multidimensional defect potential: in two dimensions the lowest part of the saddle point that defines the barrier height need not be collinear with the local minima of the double-well potential, so the height of both barriers can be, for example, lowered by the same sign bias. Thus these defects are not necessarily jumping along a straight line. Clearly, the concept of effective valence is not particularly useful in a real, three-dimensional sample, because it assumes knowledge about the shape of the defect potential. But effective valence is supposed to be a means of simplifying the problem by removing all reference to the defect potential. Particularly in strongly interacting defect systems such as we observe, there is no reason why the defect potential can be treated as one dimensional.

B. Random energy term

A nontrivial random energy input to the defect fluctuations such as we observe, which is bias induced but not simple Ohmic heating, has, to our knowledge, not been previously discussed in electromigration studies. Such a term must exist, however, even within the ballistic model: the electrons transfer momentum to the defect, and naturally some energy is absorbed by the defect as well. This random energy term may well be irrelevant to electromigration processes in typical bias ranges for polycrystalline thin-film resistors (we will return to this point at the end of the paper), for at low voltages it appears to be quadratic in voltage. We present a simple model of electron heating of the defects that reproduces all of the qualitative features of the data and quite successfully fits the high- and low-temperature regimes. The effective defect temperature is calculated in two steps. First, a characteristic ‘‘temperature’’ of the nonequilibrium electron distribution is calculated as a function of sample bias, by finding the temperature that a defect equilibrates to when coupled only to the electrons. Next, the actual defect temperature T_d is estimated by finding the steady-state temperature which the defect attains when it is coupled both to the electrons at temperature T_{el} and the lattice at temperature T .

To find the electron ‘‘temperature,’’ we model the system as a free-electron-gas scattering via a point-particle interaction off a defect that has local harmonic-oscillator modes, so that the interaction Hamiltonian is given by

$$H_{\text{int}} = \delta^3(\mathbf{r} - \mathbf{x}), \quad (11)$$

where \mathbf{r} is the spatial coordinate for the defect wave function, and \mathbf{x} is the spatial coordinate for the electron wave function. Then the matrix element between an initial state of the electron with wave vector \mathbf{k} and the defect in

state $|i\rangle$, and a final state of the electron with wave vector \mathbf{k}' and the defect in state $|f\rangle$, is

$$M = (\text{volume})^{-1} \langle i | e^{i\mathbf{Q}\cdot\mathbf{r}} | f \rangle, \quad (12)$$

where $\mathbf{Q} = \mathbf{k}' - \mathbf{k}$.

Using Fermi's golden rule, the transition rate is then given by

$$\Gamma_{\mathbf{k}-\mathbf{k}', i \rightarrow f} = \frac{2\pi}{\hbar} |M|^2 f_{\mathbf{k}} (1 - f_{\mathbf{k}'}) \delta(E_f - E_i + E_{\mathbf{k}} - E_{\mathbf{k}'}), \quad (13)$$

where $f_{\mathbf{k}}$ is the electron distribution function. Lovesy¹⁸ gives the scattering function for particles colliding with a harmonic oscillator at finite temperature. He finds

$$\begin{aligned} S(\mathbf{Q}, \hbar\omega) &\equiv \sum_{i,f} p_i |\langle i | e^{i\mathbf{Q}\cdot\mathbf{r}} | f \rangle|^2 \delta(\hbar\omega + E_i + E_f) \\ &= e^{-2W} \sum_{n=-\infty}^{\infty} I_n(y) e^{\beta_d(\hbar\omega/2)n} \delta(\hbar\omega - n\hbar\omega_d), \end{aligned} \quad (14)$$

where

$$\begin{aligned} W &= \frac{\hbar Q^2}{4\omega_d m_d} \coth \left[\frac{\hbar\omega_d}{2kT_d} \right], \\ y &= \frac{\hbar Q^2}{2\omega_d m_d} \operatorname{cosech} \left[\frac{\hbar\omega_d}{2kT_d} \right], \end{aligned} \quad (15)$$

and I_n is a modified Bessel function of the first kind. Thus the net power absorbed by the defect from the electrons, including transitions in which the electrons absorb energy from the defect, is given by

$$P \propto \sum_{\mathbf{k}, \mathbf{k}'} (E_{\mathbf{k}} - E_{\mathbf{k}'}) f_{\mathbf{k}} (1 - f_{\mathbf{k}'}) S(\mathbf{Q}, E_{\mathbf{k}} - E_{\mathbf{k}'}). \quad (16)$$

In a ballistic point contact the electron distribution function as a function of voltage is well known.¹⁴ For the particular case of electrons at the center of the device,

$$f_{\mathbf{k}} = \begin{cases} \frac{1}{e^{\beta[E_{\mathbf{k}} - (\epsilon_F + eV/2)]} + 1}, & k_z > 0 \\ \frac{1}{e^{\beta[E_{\mathbf{k}} - (\epsilon_F - eV/2)]} + 1}, & k_z < 0 \end{cases} \quad (17)$$

where z refers to the direction of current flow. The effective electron temperature is determined by integrating Eq. (16) numerically and adjusting the effective defect temperature T_d until the net power absorbed by the defect is zero. We have also computed the effective electron temperature both at the center of the constriction and away from the center. These calculations show that we can account for the defect being in a location other than the center of the device simply by scaling the maximum effective electron temperature $T_{\text{el,max}}$ (that found in the center) by

$$T_{\text{el}} = (T_{\text{el,max}} - T) / s + T, \quad (18)$$

where $s \geq 1$ is a scaling factor that reflects the location of the defect in the device. Equation (18) is a statement of the fact that the amount of "heating" of the electrons above the lattice temperature is, to a very good approximation, proportional to the phase space available for scattering. Over the range of experimental voltages, this approximation introduces no more than 1% error.

The temperature of a defect in equilibrium with the electrons is independent of the particular details of the vibrational modes of the defect; in a sense the defect is merely acting as a thermometer for the electrons. However, at low temperatures the defect cannot equilibrate with the electrons until the electrons have enough energy to excite the first-excited state of the defect. This means that at low voltages and temperatures there will be some variation in the value of T_{el} calculated, depending on the particular choice of defect model. The low-voltage measurements of defect fluctuations have been conducted primarily at high enough temperatures that thermal smearing removes much of this difference. Nonetheless, as a reasonable choice we take the defect to be localized in a harmonic-oscillator potential characterized by a frequency ω_d , which we expect to be of order 10^{13} sec.

Using the values of τ_0 , ϵ , and ζ obtained from the low-voltage data, we can convert the measured fluctuation times into effective temperatures, in order to compare with the results of the calculation. Figure 8 shows T_d of a defect fluctuation along with the calculated electron "temperature" as a function of voltage at a lattice temperature of 98 K. We find the measured defect temperature T_d smaller than the calculated electron "temperature" T_{el} for all the defect fluctuations studied, with essentially no adjustable parameters. This is, of course, to be expected. Not only have we calculated the maximum electron "temperature," but the defect can lose energy to the lattice, and should lie at a temperature some-

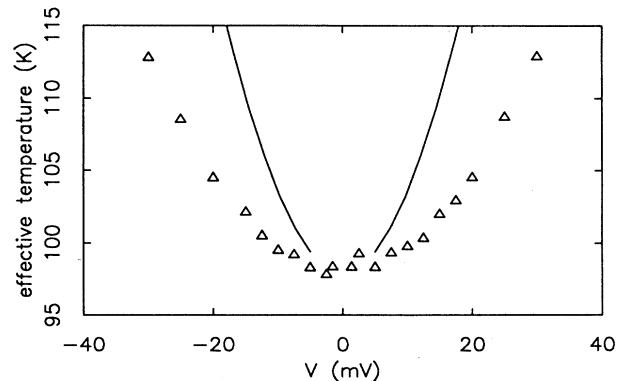


FIG. 8. Calculated electron "temperature" as a function of voltage at a lattice temperature of 100 K (solid line) compared to the measured defect temperature (triangles) for a defect fluctuation in an aluminum nanobridge. Because the defect is also coupled to the lattice, which is at a lower temperature than the electrons, the electron "temperature" is always higher than the defect temperature.

where between that of the electrons and that of the lattice. At low temperatures T_{el} is much higher than T_d , and cannot be plotted in the same figure as the actual data. As shown in Fig. 9, however, T_{el} does reproduce the temperature-independent behavior that is observed at low temperatures (see Fig. 6).

Although we have not done a detailed calculation to include the coupling of the defect to the lattice, we present arguments for the expected behavior at low voltages, where $T_{el} \sim T$, and at low temperatures, where $T_{el} \gg T$. When T_d is not much different from that of its surroundings, we can do a Taylor-series expansion of the relaxation rate of the defect temperature towards the electron and lattice temperatures, so that

$$-\frac{dT_d}{dt} = \gamma_{el}(T_d - T_{el}) + \gamma_{ph}(T_d - T), \quad (19)$$

where γ_{el} and γ_{ph} are constant energy relaxation rates of the defect to the electrons and the lattice, respectively. Under steady-state conditions $dT_d/dt = 0$, so in the range of validity of Eq. (19), when $T_{el} \sim T$, we expect

$$T_d = \frac{\gamma_{el}}{\gamma_{el} + \gamma_{ph}}(T_{el} - T) + T. \quad (20)$$

When we measure $T_d \gg T$, the lattice temperature clearly cannot influence the rate of relaxation of energy from the defect to the lattice. If the lattice temperature is low enough that not many phonons are present, the defect does not absorb appreciable energy from the lattice, and the probability of the defect relaxing by emitting a phonon is independent of the lattice temperature. If we again assume a single relaxation rate from the defect to each reservoir, when $T_d \gg T$, we expect the $T=0$ result of Eq. (20),

$$T_d = \frac{\gamma_{el}}{\gamma_{el} + \gamma_{ph}} T_{el}. \quad (21)$$

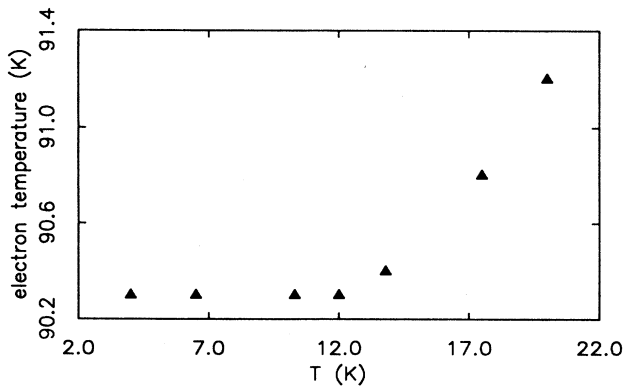


FIG. 9. Calculated electron "temperature" at 19 mV as a function of lattice temperature. The electron temperature becomes independent of lattice temperature at low T , which explains why the measured defect fluctuation rate becomes independent of temperature at low temperature (Fig. 6).

Defining $\alpha = (\gamma_{el} + \gamma_{ph})/\gamma_{el}$, Eq. (20) can be rewritten

$$T_d = \frac{T_{el}}{\alpha} + T \left[1 - \frac{1}{\alpha} \right], \quad (22)$$

and Eq. (21) becomes

$$T_d = \frac{T_{el}}{\alpha}. \quad (23)$$

In order to compare the calculation with the data, we adopt a simple function to interpolate between the two regimes,

$$T_d = \frac{T_{el}}{\alpha} + T \left[1 - \frac{1}{\alpha} \right] \frac{T}{T_{el}}. \quad (24)$$

Naturally, we do not expect perfect agreement between the data and the calculation in between the limits $(T_d - T)/T \ll 1$ and $(T_d - T)/T \gg 1$.

By varying the parameter s of Eq. (18) and α of Eq. (24), we can fit the measured defect temperature quite successfully, as is shown in Fig. 10 for a defect fluctuation in an aluminum nanobridge. The interpolation scheme works remarkably well, indicating that a single value of α , which reflects the relative coupling of the defect to the electrons and to the lattice, does indeed explain both the high- and low-temperature behavior of the data. Table I lists measured values of α for the various defect fluctuations studied. (For the defect in palladium, data were not available in the low-temperature regime, so a value of s could not be determined. The value of α listed in the table assumes this defect is in the center of the device, so $s = 1$. When this value of s is chosen, the resulting fit produces a value of α that is also similar to that found for the defects in the other materials.) The relative coupling of the defect to the electrons and the lattice is quite uni-

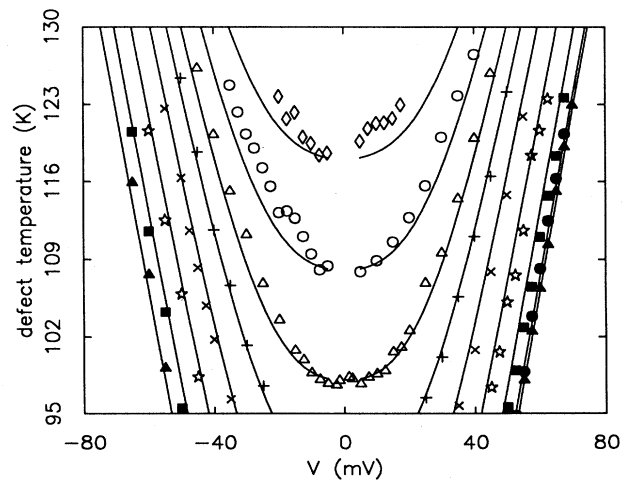


FIG. 10. Measured defect temperature for a defect fluctuation in an aluminum nanobridge at several temperatures: \diamond , $T = 118$ K; \circ , $T = 108$ K; \triangle , $T = 98$ K; $+$, $T = 89$ K; \times , $T = 77$ K; \star , $T = 60$ K; \blacksquare , $T = 39$ K; \bullet , $T = 19$ K; \blacktriangle , $T = 4$ K. The fit to the data is discussed in the text.

form from one defect to the next. We find that the relaxation rate of energy from the defect to the lattice is comparable to and slightly smaller than the relaxation rate of energy from the defect to the electrons. The difference in α for a defect in each of its two configurations is statistically significant, and proves that the effective defect temperature is not simply due to overall sample heating, again because the same defect is heated to a different effective temperature in each of its two configurations. Also listed in Table I are the values of ω_d , and the location of the defect relative to the center of the device that is implied by the value of s used in the fit, assuming that the defect lies on the axis of symmetry of the device. Defect locations range from $z \sim 0$ to $z \sim 1.3a$, where a is the constriction radius. Not surprisingly, some of the defects studied happened to be located away from the center of the device. If the defects are off the axis of symmetry of the device, their distance from the center is smaller.

VI. SUMMARY

In summary, we have observed electromigration processes directly in thin-film metal samples so small that individual defect motion causes a measurable resistance change. True electromigration, in which the sample resistance changes permanently, is the result of these processes acting on the entire "defect glass" that best describes the strongly interacting defects in these clean thin-film samples, leading to a very complex electromigration behavior. By studying the dynamics of reversible two-level defect fluctuations, we have obtained quantitative measurements of the electromigration behavior of individual defects in copper, aluminum, and palladium thin films. This electromigration behavior is dominated by inelastic electron-defect scattering that preferentially heats the defects above the lattice temperature, enhancing the rate at which electromigration occurs, with the smaller, expected, electromigration force term providing the

overall bias to favor net atomic motion. These results for high-field, high-current-density transport are relevant not only to the metal nanobridges in which we have observed them; an electron-heating term in which electrons transfer energy to oxide defects has, in fact, been observed in tunnel junctions with amorphous or quasiamorphous tunnel barriers.¹⁹ The switching noise that is often seen in scanning tunneling microscopy, particularly at the higher bias levels, is most likely a result of the excitation of metastable atomic-scale defects by the tunneling electrons. Indeed, these electromigration processes quite probably describe the scanning-tunneling-microscopy lithographic process in which material is transferred from the tunneling tip to the sample when a high bias is applied. In addition, it is possible that even at the lower operating biases typical for thin-film metal structures the electron-scattering rate may be high enough at grain boundaries for significant electron "heating" to occur, accelerating the electromigration- and thermal-stress-induced wearout of metalization.

ACKNOWLEDGMENTS

We wish to acknowledge the assistance of Richard Tiberio and other staff members at the National Nanofabrication Facility at Cornell University in the fabrication of the nanobridges. This research was supported by the U.S. National Science Foundation through the Cornell Materials Science Center under Grant No. DMR-85-16616 and by the U.S. National Science Foundation (NSF) through use of the National Nanofabrication Facility under Grant No. ECS-86-19049. One of us (K.S.R.) acknowledges partial financial support from AT&T Bell Laboratories, and one of us (D.C.R.) acknowledges partial support from the NSF. We wish to thank J. P. Sethna and J. D. Shore for instigating the model for the defect heating, and J. P. Sethna, J. D. Shore, and R. H. Silsbee for helpful conversations and comments on the manuscript.

¹H. B. Huntington and A. R. Grone, *J. Phys. Chem. Solid* **20**, 76 (1961).

²See references in J. C. M. Hwang and R. W. Balluffi, *Scr. Metall.* **17**, 709 (1978).

³For reviews on electromigration, see H. B. Huntington, in *Diffusion in Solids: Recent Developments*, edited by A. S. Nowick and J. J. Burton (Academic Press, New York, 1975), Chap. 6; A. H. Verbruggen, *IBM J. Res. Dev.* **32**, 93 (1988).

⁴C. Bosvieux and J. Friedel, *J. Phys. Chem. Solids* **23**, 123 (1962).

⁵A. K. Das and R. Peierls, *J. Phys. C* **6**, 2811 (1973).

⁶R. S. Sorbello, *Phys. Rev. B* **23**, 5119 (1981).

⁷R. Landauer, *IBM J. Res. Dev.* **1**, 223 (1957).

⁸V. B. Fiks, *Fiz. Tverd. Tela (Leningrad)* **1**, 16 (1959) [*Sov. Phys.—Solid State* **1**, 12 (1959)].

⁹R. S. Sorbello, *J. Phys. Chem. Solids* **34**, 937 (1973).

¹⁰T. C. Genoni and H. B. Huntington, *Phys. Rev. B* **16**, 1344 (1977).

¹¹L. Lou, W. L. Schaich, and J. C. Swihart, *Phys. Rev. B* **33**, 2170 (1986).

¹²R. P. Gupta, Y. Serruys, G. Brebec, and Y. Adda, *Phys. Rev. B* **27**, 672 (1983).

¹³A. Lodder and M. G. E. Brand, *J. Phys. F* **14**, 2955 (1984).

¹⁴I. K. Yanson and O. I. Shklyarevskii, *Fiz. Nizk. Temp.* **12**, 899 (1986) [*Sov. J. Low Temp. Phys.* **12**, 509 (1986)]; A. G. M. Jansen, A. P. Van Gelder, and P. Wyder, *J. Phys. C* **13**, 6073 (1980).

¹⁵K. S. Ralls and R. A. Buhrman, *Phys. Rev. Lett.* **60**, 2434 (1988).

¹⁶Che-Yu Li, Ronald D. Black, and William R. LaFontaine, *Appl. Phys. Lett.* **53**, 31 (1988).

¹⁷R. S. Sorbello, *Phys. Rev. B* **39**, 4984 (1989).

¹⁸S. W. Lovesey, *Condensed Matter Physics: Dynamic Correlations* (Benjamin/Cummings, Reading, MA, 1980), p. 8.

¹⁹C. T. Rogers, Ph.D. thesis, Cornell University, Ithaca, NY, 1987.